Suzaku broad band spectrum of 4U 1705–44: Probing the Reflection component in the hard state

T. Di Salvo[1]⋆, R. Iaria[1], M. Matranga[1], L. Burderi[2], A. D'Aí[1],
E. Egron[3], A. Papitto[4], A. Riggio[2], N. R. Robba[1], Y. Ueda[5]

[1] *Dipartimento di Fisica e Chimica, Università degli Studi di Palermo, via Archirafi 36 - 90123 Palermo, Italy*

[2] *Università degli Studi di Cagliari, Dipartimento di Fisica, SP Monserrato-Sestu, KM 0.7, 09042 Monserrato, Italy*

[3] *INAF – Osservatorio Astronomico di Cagliari, via della Scienza 5, 09047 Selargius (CA), Italy*

[4] *Institut de Ciéncies de l'Espai (IEEC-CSIC), Campus UAB, Fac. de Ciéncies, Torre C5, parell, 2a planta, 08193, Barcelona, Spain*

[5] *Department of Astronomy, Kyoto University, Kitashirakawa-Oiwake-cho, Sakyo-ku, Kyoto 606-8502, Japan*

ABSTRACT

Iron emission lines at $6.4 - 6.97$ keV, identified with Kα radiative transitions, are among the strongest discrete features in the X-ray band. These are one of the most powerful probes to infer the properties of the plasma in the innermost part of the accretion disk around a compact object. In this paper we present a recent *Suzaku* observation, 100–ks effective exposure, of the atoll source and X-ray burster 4U 1705–44, where we clearly detect signatures of a reflection component which is distorted by the high–velocity motion in the accretion disk. The reflection component consists of a broad iron line at about 6.4 keV and a Compton bump at high X-ray energies, around 20 keV. All these features are consistently fitted with a reflection model, and we find that in the hard state the smearing parameters are remarkably similar to those found in a previous *XMM-Newton* observation performed in the soft state. In particular, we find that the inner disk radius is $R_{in} = 17 \pm 5$ R_g (where R_g is the Gravitational radius, GM/c^2), the emissivity dependence from the disk radius is $r^{-2.5\pm0.5}$, the inclination angle with respect to the line of sight is $i = 43° \pm 5°$, and the outer radius of the emitting region in the disk is $R_{out} > 200$ R_g. We note that the accretion disk does not appear to be truncated at large radii, although the source is in a hard state at $\sim 3\%$ of the Eddington luminosity for a neutron star. We also find evidence of a broad emission line at low energies, at 3.03 ± 0.03 keV, compatible with emission from mildly ionized Argon (Ar

XVI-XVII). Argon transitions are not included in the self–consistent reflection models that we used and we therefore added an extra component to our model to fit this feature. The low energy line appears compatible with being smeared by the same inner disk parameters found for the reflection component.

Key words: line: formation — line: identification — stars: neutron — stars: individual: 4U 1705–44 — stars: magnetic fields — X-ray: general — X-ray: binaries

1   INTRODUCTION

Neutron Star Low Mass X-ray Binaries (hereafter NS LMXBs) are binary systems in which a weakly magnetic NS accretes matter from a low mass ($< 1 M_{\odot}$) companion star via Roche-Lobe overflow. In these systems the accretion disk can approach the compact object, as testified by the very fast time variability observed up to kHz frequencies (see van der Klis 2006, as a review). Broad emission lines (FWHM up to ~ 1 keV) at energies in the range $6.4 - 6.97$ keV are often observed in the spectra of NS LMXBs (e.g. Di Salvo et al. 2005; Piraino et al. 2007; Bhattacharyya & Strohmayer 2007; Cackett et al. 2008; Pandel et al. 2008; Di Salvo et al. 2009; D'Aì et al. 2009; Iaria et al. 2009; Papitto et al. 2009; Cackett et al. 2009; Shaposhnikov et al. 2009; Papitto et al. 2010; Egron et al. 2011; Piraino et al. 2012; Papitto et al. 2013; Miller et al. 2013). These lines are identified with the Kα radiative transitions of iron at different ionization states. These features are powerful tools to investigate the structure of the accretion flow close to the central source; in particular, important information can be obtained from the detailed spectroscopy of the line profile, since it is determined by the ionization state, geometry and velocity field of the reprocessing plasma. In fact, the broad iron line observed in NS LMXBs is thought to originate from reflection of the primary X-ray continuum off the inner accretion disk and the width of the line is expected to be a signature of the Keplerian motion of matter in the inner accretion disk at (mildly) relativistic velocities. In this model, the combination of Doppler effects from the high orbital velocities and Special and General relativistic effects arising from the strong gravity in the vicinity of the NS smears and shifts the reflected features. As a consequence, the line will have a characteristically broad and asymmetric profile, the detailed shape of

⋆ E-mail:tiziana.disalvo@unipa.it

which depends on the inclination and on how deep the accretion disk extends into the NS gravitational potential (e.g. Fabian et al. 1989; Matt et al. 1992).

If the origin of this line is from disk reprocessing, one would also expect the presence of other discrete features (such as emission lines and absorption edges from the most abundant elements) and a bump between 20 and 40 keV due to direct Compton scattering of the primary spectrum by the electrons in the disk. Indeed this reflection bump has been observed in the spectra of some NS LMXBs (see e.g. Barret et al. 2000; Piraino et al. 1999; Yoshida et al. 1993; Fiocchi et al. 2007; Egron et al. 2013; Miller et al. 2013), usually with reflection amplitudes (defined in terms of the solid angle $\Omega/2\pi$ subtended by the reflector as seen from the corona) lower than 0.3. In some cases an anti-correlation has been claimed between the photon index of the primary spectrum and the reflection amplitude of the reprocessed component (Zdziarski et al. 1999; Barret et al. 2000; Piraino et al. 1999), the same observed in Seyfert galaxies and galactic Black Hole (hereafter BH) candidates. This is probably caused by variations in the position of the inner rim of the disk.

The disk origin of the iron line in NS LMXBs is, however, debated in literature because of the brightness of these sources, which may cause photon pile-up and systematics in CCD spectra (Ng et al. 2010), making the detection of any asymmetry in the line profile somewhat controversial. However, a large number of simulations using a statistical model of photon pile-up to assess its impacts on relativistic disk line and continuum spectra suggest that severe photon pile-up acts to falsely narrow emission lines, leading to falsely large disk radii (Miller et al. 2010). These simulations also indicate that relativistic disk spectroscopy is generally robust against pile-up when this effect is modest. Moreover, several authors (e.g. Cackett et al. 2012; Egron et al. 2013) have shown that the CCD-based spectra from *Suzaku* and *XMM-Newton* are compatible with gas-based spectra from EXOSAT, BeppoSAX, and RXTE, demonstrating that the broad profiles seen are intrinsic to the line and not due to instrumental issues. They also report that a few BeppoSAX observations show evidence for asymmetric lines, with a relativistic diskline model providing a significantly better fit than a Gaussian line (see also Piraino et al. 1999).

Nevertheless alternatives have been proposed to explain the profiles of these features. In particular, Ng et al. (2010) propose that Compton broadening may be sufficient to explain the large width of the line. However, when self-consistently included in the fit, Compton broadening alone appears to be insufficient to explain the observed line profile (see e.g. Reis et al. 2009; Egron et al. 2013; Sanna et al. 2013). Also, Cackett & Miller (2013) have

explored the observational signatures expected from broadening in a wind. In this case the iron line width should increase with increasing the column density of the absorber (due to an increase in the number of scatterings). They show that there is no significant correlation between line width and column density, favoring an inner disk origin for the line broadening rather than scattering in a wind.

4U 1705–44 is a well-studied atoll source (see Hasinger & van der Klis 1989; Olive et al. 2003), which also shows type-I X-ray bursts. Similarly to X-ray binaries containing BHs, this source regularly shows state transitions: from a high/soft state, where the X-ray spectrum is dominated by soft spectral components with typical temperatures less than a few keV, to low/hard states where the X-ray spectrum is dominated by a hard thermal Comptonisation (e.g. Barret & Olive 2002; Piraino et al. 2007). The presence of broad discrete features in this source has been often reported in literature. A broad iron line was observed, in the soft and/or hard state, with moderate/high spectral resolution by the Chandra/HETG (Di Salvo et al. 2005), BeppoSAX (Piraino et al. 2007), Suzaku (Reis et al. 2009), and XMM/pn (Di Salvo et al. 2009; D'Aì et al. 2010; Egron et al. 2013). The XMM observation, taken in August 2008 during a soft state (45 ks effective exposure time), showed one of the highest signal-to-noise ratio iron line profile ever observed in a NS LMXB. The line profile is clearly broad and could be fitted equally well with a relativistic line profile, such as *diskline* (Fabian et al. 1989) or *relline* (Dauser et al. 2010), or with self-consistent reflection models, such as *reflionx* (Ross & Fabian 2005), *refbb* (Ballantyne 2004), and *xillver* (García & Kallman 2010). All these models gave parameters of the inner disk with unprecedented precision and all compatible with each other within the small statistical uncertainties (see Di Salvo et al. 2009; D'Aì et al. 2010; Egron et al. 2013). The line is identified with the Kα transition of highly ionised iron, Fe XXV; the inner disk radius is $R_{in} = 14 \pm 2$ R$_g$ (where R$_g$ is the Gravitational radius, GM/c^2), the emissivity index of the disk is -2.27 ± 0.08 (compatible with a disk illuminated by a central source), the inclination angle with respect to the line of sight is $i = 39 \pm 1$ degrees. This, together with the presence of other low-energy features from S XVI, Ar XVIII, Ca XIX and a smeared iron edge at 8.4 keV, which all are compatible with being smeared with the same inner disk parameters, makes 4U 1705–44 the best source for a detailed spectroscopic study, in order to address the disk origin of the observed iron line and of the whole reflection component.

In this paper we present a high statistics, 100-ks effective exposure, *Suzaku* observation of 4U 1705–44 during a hard state: these data allow us a detailed study of the reflection

features and the fit, with a self-consistent reflection model, of both the iron line profile and the associated Compton reflection bump at energies above 10 keV. In this spectrum, which includes hard-band data (up to 200 keV), the overall fractional amount of reflection is well determined by fitting the Compton bump. We can therefore test whether the observed iron line is consistent with this fractional amount of reflection. In this way we confirm independently (fitting a different spectral state and using different instruments) the inner disk parameters already obtained with *XMM-Newton* in the soft state.

2 OBSERVATIONS

Suzaku (Mitsuda et al. 2007) observed 4U 1705–44 on 2012 March 27 as the result of a Target of Opportunity (ToO) program during a hard state for a total observing time of 250 ks, corresponding to an effective exposure time of about 100 ks because of observational gaps caused by Earth occultations along the low equatorial orbit of the *Suzaku* satellite. Both the X-ray Imaging Spectrometers (XIS, 0.2-12 keV; Koyama et al. (2007)) and the Hard X-ray Detector (HXD, 10-600 keV; Takahashi et al. (2007)) instruments were used during these observations. There are four XIS detectors, numbered as 0 to 3. XIS0, XIS2 and XIS3 all use front-illuminated CCDs and have very similar responses, while XIS1 uses a back-illuminated CCD. At the time of this observation the available CCDs were three due to the loss of the XIS2. The HXD instrument consists of two types of collimated (non-imaging) detectors, the PIN diodes (10-70 keV) and the GSO scintillators (30-600 keV).

We reprocessed the data using the *aepipeline* tool provided by *Suzaku FTOOLS version 20* updated with the latest calibration files (2013 November). As second step, in order to obtain a more accurate estimate of the *Suzaku* attitude, we have calculated a new attitude using the free tool *aeattcor.sl* created by J. E. Davis. Then we have applied the new attitude to XIS event files using the FTOOLS *xiscoord*. During the observation, XIS0, XIS1, and XIS3 were operated using the 1/4 window option. The effective exposure time of each XIS CCD is 96.67 ks. In order to estimate the pile-up in the XIS spectra we have used the public available tool *pile-estimate.sl* created by M. A. Novak. Using a circular region with radius equal to $105''$, we have found that in each XIS CCD, the pile-up fraction is $\sim 3\%$ at most. The pile-up fraction is sufficiently small that we can neglect its effects on our spectral fitting results. In fact, we have checked that spectral results do not change significantly if we exclude a central circle in the extraction region in order to further reduce the pile-up

fraction. Therefore, we have extracted the source and background spectra from a circular extraction region of radius 105″ each, the background circle being centered close to the edge of the CCD, where no significant contaminating photons from the source were present. The response files of each XIS spectrum have been generated using the *xisrmfgen* and *xisarfgen* tools. Since the response of XIS0 and XIS3 are very similar, we have combined their spectra and responses using the tool *addascaspec*.

The PIN spectrum has been extracted using the tool *hxdpinxbpi*. Both the non X-ray and cosmic X-ray backgrounds are taken into account. The non X-ray background (NXB) is calculated from the background event files distributed by the HXD team. The cosmic X-ray background (CXB) is from the model by Boldt & Leiter (1987). The response files provided by the HXD team are used. We selected the HXD/PIN events in the energy range 12-30 keV and produced the HXD/PIN background-subtracted light curve using the SUZAKU tool `hxd-pinxblc` and adopting the background event files distributed by the HXD team. Since this light curve follows the XIS0 light curve, we conclude that no contaminating flare was present in the data. We have also extracted the GSO spectrum running the tool *hxdgsoxbpi*. For the background we have used the 'tuned' non X-ray background, whereas for the response file we have used the latest version provided on 2011-06-01.

We have extracted the XIS0 light curves in the energy range $0.9 - 2.8$, $2.8 - 10$ and $0.9 - 10$ keV, respectively (see Fig. 1). Nine type-I X-ray bursts are observed in the total 250-ks light curve. The source (persistent) count rate gradually increases by about 40% during the observation. Since no changes are observed in the hardness ratio (given by the ratio of the source counts in the $2.8 - 10$ keV range to the source counts in the $0.9 - 2.8$ keV, see Fig. 1) we conclude that the X-ray spectral shape of the source does not change significantly during the observation.

3   SPECTRAL ANALYSIS AND RESULTS

In order to extract spectra for the persistent emission, we have excluded the type-I bursts that occurred during the observation. In particular we have excluded approximately 100 s of data starting from the onset of each burst. We adopt $0.7 - 11$ keV energy range for the XIS0+XIS3 (hereafter XIS03) and XIS1 spectra, $15 - 50$ keV energy range for the HXD/PIN spectrum and $50 - 200$ keV energy range for the HXD/GSO spectrum. We excluded the energy interval between 1.7 and 2.0 keV from the XIS03 and XIS1 spectra because of the
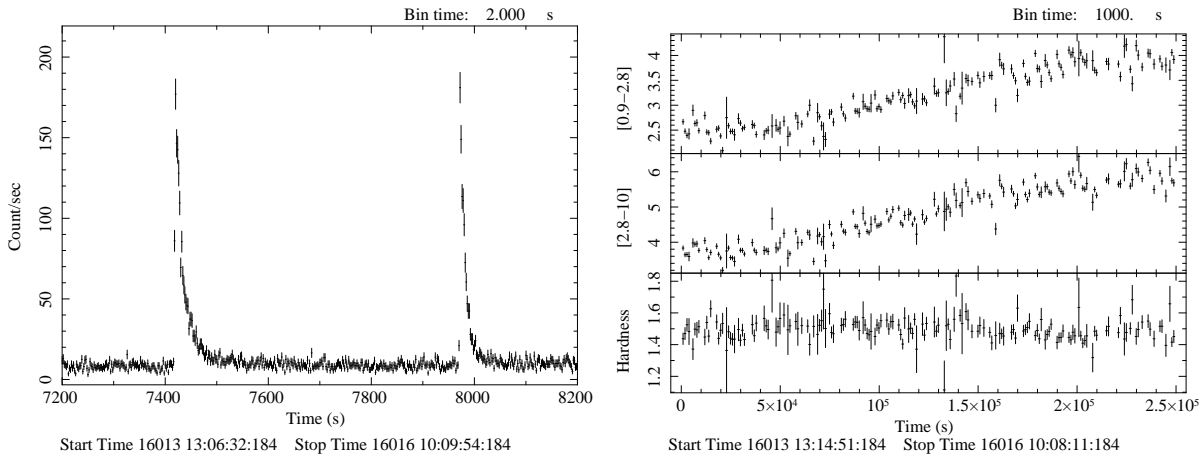
Figure 1. Left: *Suzaku* XIS0 light curve in the energy range 0.9 - 10 keV showing two of the nine type-I bursts which occurred during the 250-ks observation. **Right:** *Suzaku* XIS0 light curves in the energy range $0.9 - 2.8$ keV (top panel), $2.8 - 10$ keV (middle panel), and the corresponding hardness ratio (bottom panel).

presence of systematic features associated with neutral silicon and neutral gold which give a mismatch between the two spectra. The XIS spectra were grouped by a factor 4 in order not to oversample too much the instrumental energy resolution. The HXD/PIN and HXD/GSO spectra were grouped in order to have at least 25 photons per energy channel. We fitted the spectra using XSPEC version 12.7.0.

We started to fit the continuum in the 0.7–200 keV energy range with the typical model used for NS LMXBs of the atoll class, which revealed to be the best fit continuum for this source too (see e.g. Di Salvo et al. 2009; Piraino et al. 2007; Barret & Olive 2002). This model consists of a soft blackbody and a thermal Comptonised component, in this case modelled by `nthComp` (Życki et al. 1999), modified at low energy by photoelectric absorption caused by neutral matter and modeled by `phabs` in XSPEC. This continuum model gave, however, an unacceptable fit, corresponding to a $\chi^2/dof = 2425.13/1511$, because of the presence of evident localised residuals at 2.5–3.5 keV, 6–9 keV and 15–30 keV. The most prominent is a clear iron line profile at energies from 5 to 7 keV and an absorption feature at 7–8 keV (see Fig. 2).

In order to fit these residuals, we first added to our continuum model the `pexriv` component (Magdziarz & Zdziarski 1995) which takes into account the iron edge and Compton bump present in the residuals. Note that pexriv does not self-consistently include any emission line. The photon index and the high energy cutoff of the pexriv component were fixed to those of the nthComp component. Here and in the following we neglect any reflection of the soft (blackbody) component, which in any case contributes to a small fraction of the total flux and most of its flux is at soft energies (below $4 - 5$ keV). The addition of
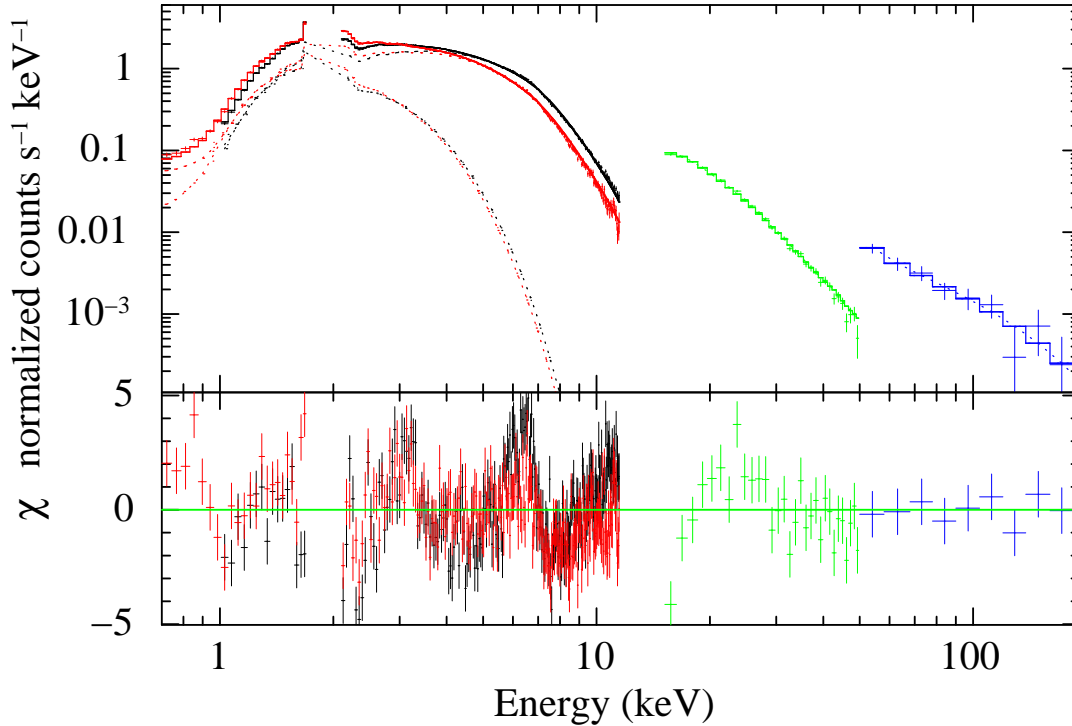
Figure 2. *Suzaku* data in the energy range 0.7 - 200 keV (top) and residuals in units of σ with respect to the simpler phenomenological model (bottom) of 4U 1705–44. The model consists of a blackbody (dotted lines) and the Comptonization component *nthComp*, both multiplied by photoelectric absorption.

this component gave a significant improvement of the fit reducing the χ^2/dof to the value 2009.67/1509 ($\Delta\chi^2 = 415$ for the addition of two parameters). Therefore, the presence of the Compton hump and the iron edge are detected with high statistical significance (an F-test would give a probability of chance improvement of the fit negligibly small, $\sim 2.7 \times 10^{-62}$). We then added a Gaussian line at 6.4 keV obtaining again an improvement of the fit. As a first step we decided to fix the energy of the line at 6.4 keV because, otherwise, it tends to get broad (Gaussian sigma about 1 keV) and its energy tends to decrease to 6.2 keV. This fit gives a $\chi^2/dof = 1956.50/1507$ ($\Delta\chi^2 = 53$ for the addition of two parameters). This line can be identified with fluorescence from neutral iron. The addition of another Gaussian at about 3 keV again improves the fit, giving $\chi^2/dof = 1829.89/1504$ ($\Delta\chi^2 = 127$ for the addition of three parameters). This line can be identified with emission from mildly ionized Argon, Ar XVI–XVII. In order to check whether the iron line energy was stable or not, we let the iron line energy free to vary obtaining $\chi^2/dof = 1818/1503$. We also tried to substitute the Gaussian line at ~ 6 keV with a diskline. In this case we had to fix all the smearing parameters but the inner radius of the disk. This did result in a slight improvement

Table 1. The best fit parameters of the spectral fitting of the *Suzaku* spectrum of 4U 1705–44 in the $0.7 - 200$ keV energy range with phenomenological models. The blackbody luminosity is given in units of L_{35}/D_{10}^2, where L_{35} is the bolometric luminosity in units of 10^{35} ergs/s and D_{10} the distance to the source in units of 10 kpc. The blackbody radius is calculated in the hypothesis of spherical emission and for a distance of 7.4 kpc. Fluxes in the nthComp and pexriv components are calculated in the $1 - 16$ keV range, while total flux is calculated in the $1 - 10$ keV band. Uncertainties are given at 90% confidence level.

Component	Parameter	Basic Model	Pexriv	Pexiriv + 2Gauss	Smeared (Pex + 2Gaus)
phabs	N_H ($\times 10^{22}$ cm^{-2})	1.899 ± 0.025	2.13 ± 0.05	2.02 ± 0.05	2.04 ± 0.06
bbody	kT_{BB} (keV)	0.503 ± 0.015	$0.265^{+0.004}_{-0.026}$	0.39 ± 0.04	0.35 ± 0.04
bbody	L_{BB} (L_{35}/D_{10}^2) / Norm	8.8 ± 0.6	3.6 ± 0.8	5.3 ± 1.3	4.0 ± 0.6
bbody	R_{BB} (km)	7.6 ± 0.5	17.6 ± 4.4	9.8 ± 2.3	10.6 ± 2.5
nthComp	kT_{seed} (keV)	0.90 ± 0.04	0.569 ± 0.014	0.69 ± 0.06	0.64 ± 0.04
nthComp	Γ	2.05 ± 0.03	2.081 ± 0.018	2.05 ± 0.04	2.08 ± 0.03
nthComp	kT_e (keV)	101^{+100}_{-74}	$63.2^{+12}_{-2.4}$	$80.7^{+59}_{-9.9}$	89^{+28}_{-20}
nthComp	Flux (10^{-10} ergs cm^{-2} s^{-1})	4.73	4.67	4.66	4.61
pexriv	ξ (erg cm s^{-1})	$-$	< 1	< 1	< 1
pexriv	Incl (deg)	$-$	40 (fixed)	40 (fixed)	40 (fixed)
pexriv	Flux (10^{-10} ergs cm^{-2} s^{-1})	$-$	0.9	0.56	0.73
gauss	E_{line} (keV)	$-$	$-$	3.00 ± 0.04	3.02 ± 0.04
gauss	σ_{line} (keV)	$-$	$-$	0.28 ± 0.03	$-$
gauss	I_{line} ($\times 10^{-4}$ ph cm^{-2} s^{-1})	$-$	$-$	3.3 ± 0.9	2.4 ± 0.5
gauss	EqW (eV)	$-$	$-$	24.0 ± 7.6	18.3 ± 3.5
gauss	E_{Fe} (keV)	$-$	$-$	6.21 ± 0.08	6.27 ± 0.06
gauss	σ_{Fe} (keV)	$-$	$-$	0.46 ± 0.07	$-$
gauss	I_{line} ($\times 10^{-4}$ ph cm^{-2} s^{-1})	$-$	$-$	$1.58^{+1.2}_{-0.19}$	$1.9^{+0.7}_{-0.4}$
gauss	EqW (eV)	$-$	$-$	33 ± 17	52 ± 21
rdblur	*Betor*	$-$	$-$	$-$	-2.2 ± 0.5
rdblur	R_{in} (GM/c^2)	$-$	$-$	$-$	< 29
rdblur	R_{out} (GM/c^2)	$-$	$-$	$-$	360^{+360}_{-160}
rdblur	Incl (deg)	$-$	$-$	$-$	54^{+17}_{-9}
total	Flux (10^{-10} ergs cm^{-2} s^{-1})	3.3 ± 0.7	3.34 ± 0.02	3.34 ± 0.03	3.34 ± 0.03
total	χ^2 (dof)	2425 (1511)	1990 (1509)	1818 (1503)	1783 (1501)

of the fit, since we get $\chi^2/dof = 1803/1503$ fixing the emissivity index at -2.4, the outer radius at 400 R$_g$, the inclination angle at 40 deg. Also in this case the centroid energy of the line remained at $6.1 - 6.3$ keV, but we get an upper limit to the inner radius of the disk of 25 R$_g$. On the other hand, we get a more significant improvement of the fit if we add a (mild) relativistic smearing to the whole reflection component (i.e. the emission lines at ~ 3 and ~ 6 keV and the pexriv component) convolving all these three components with `rdblur`, the kernel of `diskline`. In this case we get $\chi^2/dof = 1783/1501$ ($\Delta\chi^2 = 35$ for the addition of three parameters, corresponding to an F-test probability of chance improvement of $\sim 4 \times 10^{-7}$). The results of these phenomenological models are reported in Table 1.

In order to fit the high-quality *Suzaku* spectrum with more consistent physical models, we substitute the pexriv + Fe line components with the self-consistent reflection model `reflionx` (Ross & Fabian 2005), modified by a relativistic blurring component (again modeled with rdblur) to consider the relativistic and/or Doppler effects produced by the motion in the inner disk close to the compact object. In this model, emission lines from the most abundant elements or ions are also self-consistently calculated. In the reflionx model the

Table 2. The best fit parameters of the spectral fitting of the *Suzaku* spectrum of 4U 1705–44 in the $0.7 - 200$ keV energy range with the self-consistent reflection model `reflionx`. The blackbody luminosity is given in units of L_{35}/D_{10}^2, where L_{35} is the bolometric luminosity in units of 10^{35} ergs/s and D_{10} the distance to the source in units of 10 kpc. The blackbody radius is calculated in the hypothesis of spherical emission and for a distance of 7.4 kpc. The disk blackbody normalization is given by $(R_{in}(km)/D_{10})^2 \cos i$, where i is the inclination angle of the binary system. The disk blackbody inner radius R_{in} (km) is calculated for an inclination angle of $40°$. Flux is calculated in the $1 - 10$ keV band. Uncertainties are given at 90% confidence level.

Parameter	BBODY [Fe = 1]	DISKBB [Fe = 1]	BBODY [Fe = 2]	DISKBB [Fe = 2]
N_H ($\times 10^{22}$ cm^{-2})	2.11 ± 0.04	2.27 ± 0.04	2.09 ± 0.04	2.25 ± 0.04
kT_{BB} (keV)	0.38 ± 0.03	0.53 ± 0.07	0.38 ± 0.03	0.52 ± 0.08
L_{BB} (L_{35}/D_{10}^2) / Norm	5.5 ± 0.7	58 ± 22	4.9 ± 0.5	61^{+42}_{-18}
R_{BB} (km) / R_{in} (km)	10.6 ± 1.8	6.4 ± 1.2	10.0 ± 1.7	$6.6^{+2.3}_{-1.0}$
kT_{seed} (keV)	0.68 ± 0.03	0.70 ± 0.06	0.66 ± 0.03	0.67 ± 0.06
Γ	2.01 ± 0.02	2.01 ± 0.02	1.95 ± 0.01	1.95 ± 0.01
kT_e (keV)	47^{+19}_{-11}	47^{+17}_{-10}	27 ± 5	27 ± 5
ξ (erg cm s^{-1})	< 13	< 19	< 24	22 ± 4
Betor	-2.5 ± 0.5	-2.5 ± 0.5	-2.4 ± 0.4	-2.5 ± 0.5
R_{in} (GM/c^2)	17^{+4}_{-6}	16^{+4}_{-7}	16^{+4}_{-5}	16^{+4}_{-7}
R_{out} (GM/c^2)	370^{+8000}_{-180}	370^{+370}_{-170}	330^{+8000}_{-200}	350^{+350}_{-170}
Incl (deg)	43 ± 5	42 ± 5	41 ± 4	42 ± 4
E_{line} (keV)	3.03 ± 0.03	3.03 ± 0.03	3.04 ± 0.03	3.04 ± 0.03
I_{line} ($\times 10^{-4}$ ph cm^{-2} s^{-1})	2.4 ± 0.4	2.3 ± 0.4	2.4 ± 0.4	2.3 ± 0.4
EqW (eV)	18.2 ± 3.6	17.0 ± 3.4	18.6 ± 3.5	17.5 ± 3.7
Flux (10^{-10} ergs cm^{-2} s^{-1})	3.34 ± 0.04	3.34 ± 0.15	3.34 ± 0.04	3.34 ± 0.14
total χ^2 (dof)	1831 (1503)	1841 (1503)	1846 (1503)	1852 (1503)

emergent (reflected) spectrum is calculated for an optically-thick atmosphere (such as the surface of an accretion disk) of constant density illuminated by radiation with a power-law spectrum, whose photon index is fixed to that of the nthComp component, and a high-energy exponential cutoff with e-folding energy fixed at 300 keV. In order to take into account the high-energy cutoff in the illuminating spectrum, we have multiplied the reflionx spectrum by a high energy cutoff with the e-folding energy fixed to the value of the e-folding energy of the primary (nthComp) component. Since the reflionx model does not take into account transitions from Ar and Ca, we fitted the emission line at ~ 3 keV with a diskline, fixing all the smearing parameters to those used for the reflionx component. The continuum emission is fitted with the same model as before, and we used for the soft component alternatively the bbody or the diskbb model. The results of these fits are shown in Table 2. We also checked the possibility of iron overabundance with respect to cosmic abundances (as claimed by Egron et al. 2013, for the soft state), fixing the iron abundance alternatively to the cosmic value and twice the cosmic value. We find a slightly better fit when we fix the iron abundance to the cosmic value and we use a blackbody to fit the soft thermal component (see Table 2). The total $0.5 - 200$ keV luminosity of the source during the *Suzaku* observation was 6.15×10^{36} ergs/s assuming a distance to the source of 7.4 kpc.

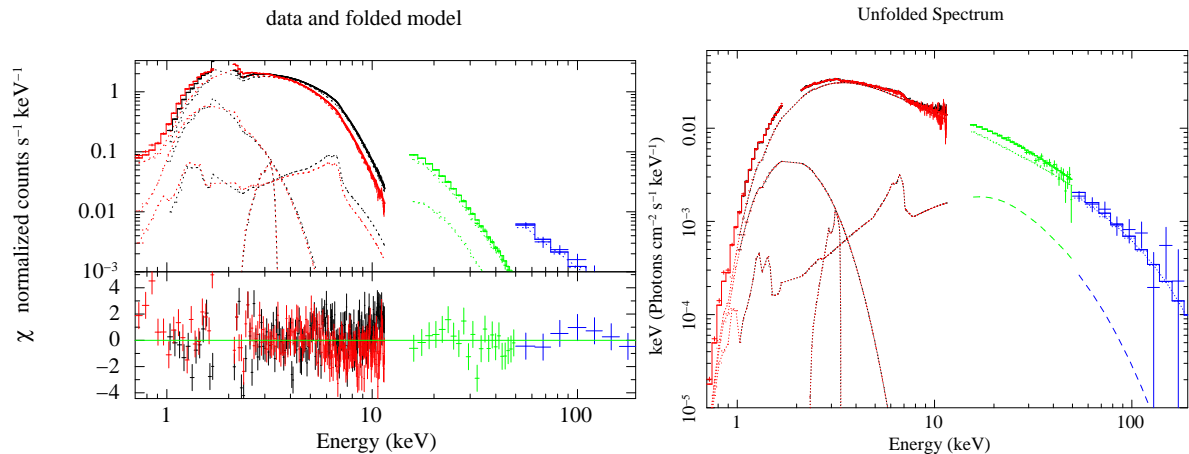Finally, we fitted the reflection component in the *Suzaku* spectrum of 4U 1705–44 with the

Figure 3. Left: *Suzaku* data in the energy range 0.7 - 200 keV (top) and residuals in units of σ with respect to the best-fit model (bottom) of 4U 1705–44 (see Table 2, first column). **Right:** *Suzaku* unfolded spectrum in the energy range 0.7 - 200 keV with respect to the best-fit model shown in the first column of Table 2. The model components are also shown. From the left to the right we see the blackbody component, the emission line at $\sim$ 3 keV (smeared with the same smearing parameters used for the reflection component), the smeared reflection component modeled by *reflionx*. The main Comptonization component and the total model are plotted on top of the data.

convolution model `rfxconv` (Kolehmainen et al. 2011), which has the advantage to take into account the exact shape of the illuminating continuum. For sake of completeness we also tried the self-consistent reflection model `relxill` by García et al. (2014), whose novelty is that for each point on the disk the proper reflection spectrum is chosen for each relativistically calculated emission angle. In the relxill model we fixed the photon index and e-folding energy of the reflected spectrum to those of the nthComp component. Both these models include emission lines from the most abundant elements or ions, as in the case of `reflionx`. Again we obtain a good fit of the 4U 1705–44 spectrum, with best-fit values of the reflection and smearing parameters well in agreement with those obtained with other reflection models (see Tab. 3, cf. with Tab. 1 and 2).

4   DISCUSSION

Similar to BH X-ray Binaries, NS LMXBs show clear differences in the spectral parameters during hard and soft states. Studying these differences is important in order to address different geometry or physical properties of the inner central emitting region in these two spectral states and in order to understand what causes the spectral transition. In fact, there is no general consensus on the hot corona–accretion disk geometry in these two spectral states. Theoretically the hard Comptonized component may come from either a patchy corona, possibly powered by magnetic flares (e.g. Beloborodov 1999) or the base of a centrally located jet (e.g. Markoff et al. 2005). In both the cases, the thin accretion disk may extend

Table 3. The best fit parameters of the spectral fitting of the *Suzaku* spectrum of 4U 1705–44 in the $0.7 - 200$ keV energy range with the self-consistent reflection models `rfxconv` and `relxill`. The blackbody luminosity is given in units of L_{35}/D_{10}^2, where L_{35} is the bolometric luminosity in units of 10^{35} ergs/s and D_{10} the distance to the source in units of 10 kpc. The blackbody radius is calculated in the hypothesis of spherical emission and for a distance of 7.4 kpc. Flux is calculated in the $0.7 - 200$ keV band. Uncertainties are given at 90% confidence level.

Parameter	RFXCONV [Fe = 1]	RELXILL [Fe = 1]
N_H ($\times 10^{22}$ cm^{-2})	2.05 ± 0.04	2.06 ± 0.05
kT_{BB} (keV)	0.37 ± 0.03	0.36 ± 0.04
L_{BB} (L_{35}/D_{10}^2) / Norm	4.6 ± 0.6	4.1 ± 0.7
R_{BB} (km) / R_{in} (km)	10.2 ± 1.8	10.3 ± 2.5
kT_{seed} (keV)	0.67 ± 0.03	0.63 ± 0.04
Γ	2.01 ± 0.01	1.979 ± 0.009
kT_e (keV)	34^{+5}_{-4}	43 ± 9
ξ (erg cm s^{-1})	60^{+20}_{-30}	12^{+9}_{-4}
Refl Amplitude	0.34 ± 0.04	0.34 (fixed)
Refl Norm	$-$	0.161 ± 0.017
Betor	-2.5 ± 0.5	$-3.2^{+0.4}_{-0.2}$
R_{in} (GM/c^2)	17^{+4}_{-7}	14 ± 2
R_{out} (GM/c^2)	> 202	260 (fixed)
Incl (deg)	43 ± 5	$31.6^{+1.9}_{-1.5}$
E_{line} (keV)	3.04 ± 0.04	3.10 ± 0.03
I_{line} ($\times 10^{-4}$ ph cm^{-2} s^{-1})	2.5 ± 0.4	2.2 ± 0.4
EqW (eV)	19.3 ± 0.3	17^{+3}_{-2}
Flux (10^{-10} ergs cm^{-2} s^{-1})	9.0 ± 0.3	$9.33^{+0.17}_{-0.36}$
total χ^2 (dof)	1832 (1503)	1818 (1504)

close to the last marginally stable orbit or the NS surface. Alternatively the thin disk may be truncated at large distances from the compact object, with the central region replaced by an advection-dominated accretion flow (ADAF) where, at high accretion rates, material may condense to form an inner optically thick disk (see e.g. Esin et al. 1997). This hot, inner flow can also act as the launching site of the jet. In this respect, much information may come from the study of the so-called reflection component in different spectral states of a source (see Done et al. 2007, as a review).

In this paper we have reported the results of the spectral analysis of a long *Suzaku* observation of the LMXB of the atoll class 4U 1705–44. This was the result of a ToO program intended to observe the source during a hard state. *Suzaku* observed the source for a total of 250 ks yielding a net exposure time of 100 ks. During the observation 9 type-I bursts were observed. We present here the spectral analysis of the persistent emission, while we will discuss the characteristics of the observed type-I bursts elsewhere. We have fitted the persistent emission spectrum in the broad band range between 0.7 and 200 keV using the continuum model which gave the best fit of previous high-quality spectra of this source obtained with RXTE, BeppoSAX, *XMM-Newton*, and Chandra (see e.g. Egron et al. 2013, and references therein). The continuum model consists of a soft component modeled

by `bbody` and a Comptonization component modeled by `nthComp`, both multiplied by the `phabs` component which takes into account photoelectric absorption by neutral matter in the interstellar medium. A smeared reflection component was necessary to obtain an acceptable fit of the broad–band *Suzaku* spectrum. This component was necessary to fit high-energy residuals above about 15 keV and a broad iron edge at about $8 - 9$ keV – the addition of the `pexriv` component to fit these two features gave a significant improvement of the quality of the fit with a probability of chance improvement, calculated with an F-test, which resulted to be negligibly small.

We detect other reflection features, such as a broad emission line at about 6.4 keV from neutral iron and a broad emission line at about 3 keV that we tentatively identify with the Kα transition from Ar XVI-XVII. These two features could be well fitted by broad `Gaussians`. Note that this Ar line is quite strong with respect to the observed iron line. If we consider the product of the element abundances ($\sim 4.7 \times 10^{-5}$ and $\sim 3.6 \times 10^{-6}$ for iron and argon, respectively) by the fluorescence yields (which can be calculated using the empirical formula yield $= Z^4/(30^4 + Z^4)$, where Z is the atomic number), we obtain $\sim 1.7 \times 10^{-5}$ and $\sim 4 \times 10^{-7}$ for iron and argon, respectively. This means that the Ar line strength should be $\sim 2.4\%$ of Fe line strength. This in the hypothesis that all the atoms of these elements are in the ionization state producing the line. Note also that the observed line may depend on the illuminating continuum at that energy. In the case of 4U 1705–44 in the soft state, where Ar and Ca lines are clearly detected by *XMM-Newton* together with an Fe line, we find small differences in the line intensities (a factor 2 at most) and higher differences in the line equivalent width (up to a factor 8). However, when the spectrum is fitted to a self-consistent reflection model, a suitably modified version of the `xillver` model by García & Kallman (2010) which includes Ar and Ca transitions, we find that the Ar line is well fitted by the reflection model with a slight overabundance by a factor 1.8 with respect to Solar abundances (see Egron et al. 2013). We conclude therefore that the simple calculation above is merely an order of magnitude estimation and that the consistency of the Ar line with other reflection features should be checked using self-consistent reflection models including Ar and Ca transitions.

We also tried to fit all the reflection features (the Compton hump, the iron edge and the iron line) with a self-consistent reflection model such as `reflionx`, which we have modified with a high energy cutoff at the electron temperature of the Comptonizing corona to take into account the curvature of the Comptonization spectrum with respect to a simple power-

Table 4. Comparison of the best-fit continuum and reflection parameters obtained for the soft state (SS) as observed in the 60-ks *XMM-Newton* observation and for the hard state (HS) observed by *Suzaku* (this paper). Continuum parameters for the SS observed by *XMM-Newton* are taken by Egron et al. (2013), who use a similar model for the continuum, while smearing parameters of the reflection component are taken from Di Salvo et al. (2009) where these parameters are obtained with smaller uncertainties. L_X is the X-ray luminosity extrapolated in the $0.1 - 150$ keV range for the SS, as reported by Egron et al. (2013), and in the $0.5 - 200$ keV range for the HS (this work). L_{Edd} is the Eddington luminosity for a 1.4 $M_\odot$ NS, $L_{Edd} = 2.5 \times 10^{38}$ ergs s^{-1} (van Paradijs & McClintock 1994).

Parameter	SS (*XMM-Newton*)	HS (*Suzaku*)
N_H ($\times 10^{22}$ cm^{-2})	2.08 ± 0.02	2.11 ± 0.04
bbody kT (keV)	0.56 ± 0.01	0.38 ± 0.03
bbody L_X (L_{37}/D_{10}^2)	2.58 ± 0.01	0.055 ± 0.007
R_{BB} (km)	33.3 ± 1.2	10.6 ± 1.8
nthComp kT_{seed} (keV)	1.30 ± 0.02	0.68 ± 0.03
nthComp kT_e (keV)	3.0 ± 0.1	47^{+20}_{-10}
ξ (erg cm s^{-1})	> 500	< 13
Betor	-2.27 ± 0.08	-2.5 ± 0.5
R_{in} (GM/c^2)	14 ± 2	17^{+4}_{-6}
R_{out} (GM/c^2)	3300^{+1500}_{-900}	370^{+8000}_{-180}
Incl (deg)	39 ± 1	43 ± 5
L_X/L_{Edd}	72%	2.9%

law (used as illuminating spectrum in the reflionx model). The smearing of the reflection component has been taken into account multiplying it by the `rdblur` component. In this case we had to add a diskline to the model to fit the Ar line at 3 keV, since transitions from Ar are not taken into account in the reflionx model. Anyway, all the smearing parameters of the diskline used to fit the Ar line have been fixed to those used for the reflection component. In this case, we used a `bbody` or a `diskbb` to fit the soft thermal component and tried to vary the iron abundance fixing this value to 1 or 2 times the cosmic abundance. The best fit corresponds to a bbody component for the soft thermal emission and to an iron abundance of 1 (see Table 2). We also tried to fit the reflection component with the self-consistent convolution model `rfxconv`, which consistently takes into account the curvature of the illuminating spectrum caused by the high-energy rollover at the electron temperature in the corona producing the primary Comptonized spectrum, or with the `relxill` model, in which the cutoff energy in the reflected spectrum is fixed at the electron temperature of the primary Comptonized component, fitted with `nthComp`. Note that both rfxconv and relxill, as well as reflionx, all include Compton broadening effects caused by Compton scattering in the surface layers of the accretion disc. The results of these fits are reported in Table 3 and are perfectly consistent with those obtained with all the other reflection models that we tried.

In order to check the stability of the best fit model with respect to the smearing parameters of the reflection component, we have let all these parameters free to vary. The

most uncertain of these parameters, as expected, is the outer radius of the disk, for which we find only loose constraints. Interestingly, all of the smearing parameters of the best fit model of this observation are in good agreement with the smearing parameters already obtained with other instruments, e.g. *XMM-Newton* and BeppoSAX (Di Salvo et al. 2009; Egron et al. 2013), during a soft state. In order to facilitate the comparison, we report in Table 4 the best fit parameters of the reflection (modeled by reflionx) and the relativistic smearing components obtained with *XMM-Newton* during a soft state (from Di Salvo et al. 2009; Egron et al. 2013) and obtained with *Suzaku* during a hard state (this paper). Although the uncertainties in the spectral parameters in the hard state are larger than in the soft state (because of the lower source flux in the hard state), we find a very good agreement in all the parameters. In particular, the inclination angles of the system we obtain in the two cases are compatible well within the 90% c.l. uncertainty. The main difference in the reflection component between the hard and the soft state is in the ionization parameter ξ, which is much larger in the soft state than in the hard state, as expected because of the higher incident flux in the soft state. Also the continuum parameters are different; in particular, the temperatures of the soft components of the continuum (i.e. of the soft blackbody component and of the seed photons for the Comptonization) result higher in the soft state, while the electron temperature of the Comptonizing cloud results higher in the hard state, in agreement with what is expected.

We note that there is no clear indication of a receding inner accretion disk radius in the hard state, corresponding to a luminosity of $\sim 3\%$ of the Eddington luminosity, with respect to the soft state, which was observed at about 70% of L_{Edd}. On the contrary, the inner disk radius as inferred from the reflection component is consistent to be the same in the two spectral states, at about 34 km from the NS center. A similar indication comes from the inner radius of the disk as inferred from the blackbody component, that we interpret as the direct emission from the accretion disk. Both in the soft and in the hard state the blackbody radius is a few tens of km, in agreement with the estimate we get from the reflection component. We caution the reader, however, that neither the color factor or the geometry of the system has been taken into account in this calculation. What is reported is just a zero-order estimation of the radius of the region (assumed to be spherical) emitting the blackbody component. In particular, the spectral hardening factor may depend on luminosity (see e.g. Merloni et al. 2000) explaining why the inner disk radius may appear larger at higher luminosities.

This result is in agreement with what is found by Egron et al. (2013) who studied *XMM-*

Newton, BeppoSAX, and RXTE spectra of 4U 1705–44 in the hard state and in the soft state. In particular, in the hard state, the inner disk radius as measured by the smearing of the reflection component resulted at $19 - 59$ R_g, which is compatible with the inner disk radius derived in the soft state (13 ± 3 R_g), while more uncertain results came from the evaluation of the blackbody radius in the hard state. D'Aì et al. (2010) also analyzed the same *XMM-Newton* observation during a hard state used by Egron et al. (2013). These authors discussed the possibility of a truncated disk in the hard state based on the best fit value of the inner disk radius as found from the Fe line width, which was about 30 R_g, that means about 60 km. However, in that case, the lack of broad–band coverage and the limited statistics, gave a large uncertainty on the inner disk radius, whose 90% c.l. range was from 6 to 90 R_g. Considering the large uncertainty on this measurement we cannot state that the result was in contrast with more recent results (Egron et al. 2013, and this work). Note also that the best-fit blackbody radius reported by D'Aì et al. (2010) has a value around 14 ± 5 km, indicating that the disk may be truncated quite close to the NS surface. Similarly, Lin et al. (2010) could not determine with high precision the inner radius of the disk using a diskline model for the Fe line in *Suzaku* and BeppoSAX spectra of 4U 1705–44 taken during a hard state. Therefore, the inner radius of the disk was fixed to 6 R_g, and the fit results, such as Fe line flux and equivalent width, were not sensitive to this parameter.

Similar results for the inner disk radius were obtained also in the case of 4U 1728–34, the prototype of the atoll sources. The *XMM-Newton* spectrum reported by Egron et al. (2011) taken during a low-luminosity state of the source (probably a hard state) showed a relatively broad iron line (Gaussian $\sigma \sim 0.6$ keV), which was fitted to a series of models (diskline, relline, and reflionx) yielding in all the cases an inner disk radius between 12 and 22 R_g. In this case a blackbody component was not significantly detected. Cackett et al. (2010) present a comprehensive, systematic analysis of *Suzaku* and *XMM-Newton* spectra of 10 NS LMXBs, in order to study their Fe $K\alpha$ emission lines. In most cases they find a narrow range of inner disk radii ($6 - 15$ R_g), implying that the accretion disk extends close to the NS surface over a range of luminosities.

In this respect, it may be useful to compare these results to those obtained for BH X-ray Binaries, since much work has been done to determine the inner radius of the disk in these systems both from the iron line and the reflection component and from the blackbody component (e.g. Done et al. 2007; Reis et al. 2010, and references therein). Also for these systems there is growing evidence that the disk may not be truncated far from the last

stable orbit. The broad-band $(0.1 - 200 \, \text{keV})$ BeppoSAX spectrum of one of the best studied galactic BH candidates, Cygnus X–1, taken during a hard state showed evidence of a complex reflection component. In this spectral deconvolution the the inner radius of the disk, as inferred from the smeared reflection, is found between 6 and 20 R_g (Di Salvo et al. 2001). This result is in agreement with the results of Young et al. (2001) who fitted ASCA, Ginga and EXOSAT data of Cygnus X–1 in both soft and hard spectral states to a model of an ionized accretion disk, whose spectrum is blurred by relativistic effects. They found that relativistic blurring provided a much better fit to the low/hard state and that data of both states were consistent with an ionized thin accretion disk with a reflected fraction of unity extending to the innermost stable circular orbit around the BH (see, however, Barrio et al. 2003, for a different interpretation). Up to date, one of the strongest evidence of a truncated disk, based on Fe line profile measurements, in a BH hard state is that of GX 339-4 (Tomsick et al. 2009). In that case, from *Suzaku* and RXTE spectra, it was found that R_{in} was a factor > 27 higher than in the bright state when the luminosity was about at 0.14% of the corresponding Eddington limit.

More recently Reis et al. (2010) have analyzed a sample of stellar mass BHs, including Cygnus X–1, in the low-hard state, down to luminosities of $\sim 10^{-3} \, \text{L}_{Edd}$, finding no clear evidence of a truncation of the inner disk at radii larger than 10 R_g. Furthermore, the thermal-disk continuum yields colour temperatures consistent with the relation $L \propto T^4$, implying that the emitting surface is consistent with being constant with luminosity. A similar relation, $L \propto T^{3.2}$, seems also to hold in the case of 4U 1705–44 at least for the soft state (Lin et al. 2010). The authors suggest that the deviation may be caused by a luminosity-dependent spectral hardening factor. On the other hand, the relatively low reflection amplitude $(\Omega/2\pi \simeq 0.34)$ we find in the hard state of 4U 1705–44 fitting its spectrum to self-consistent reflection models, such as rfxconv, is compatible with a spherical geometry with the hot (spherical) corona inside an outer accretion disk. In this case, the small inner radius of the disk we find $(\text{R}_{in} \sim 17 \, \text{R}_g$, corresponding to approximately $30 - 35$ km for a 1.4 $\text{M}_\odot$ NS) would indicate a very compact hot corona filling the central part of the accretion disk, which in the case of a NS may be identified with a boundary layer between the inner accretion disk and the NS surface. This might represent an important difference between BH and NS systems, since for a BH, in the absence of a boundary layer, the inner disk should extend down to the last stable orbit. Note, however, that alternative explanations for this weak reflection cannot be ruled out. This can be caused by a highly ionized inner

disk (e.g. Ross et al. 1999) or mildly relativistic outflow of the hot corona away from the disk (Beloborodov 1999). In the latter case, it was shown that reflection fractions as low as ~ 0.3 can be obtained in the low-hard state without invoking a truncated disk.

In summary, we have analyzed a deep (100 ks exposure time) ToO *Suzaku* observation of 4U 1705–44 during a low-luminosity hard state (corresponding to a luminosity of $\sim 3\%$ L_{Edd}). The broad-band spectrum shows a prominent Compton hump at hard energies, a Fe absorption edge and two relatively weak emission lines at ~ 3 and ~ 6.4 keV, identified with fluorescent emission from mildly ionized Ar and neutral Fe, respectively. We used all the available to date self-consistent reflection models to fit these reflection features finding in all cases best-fit parameters that are compatible with each other and consistent with those reported in literature for the soft state. In particular the inclination angles found from the reflection component for the hard and the soft state are perfectly compatible with each other. It is worth noting that we obtain similar smearing parameters in the soft and in the hard state even if in the soft state the reflection component is dominated by the Fe line, while in the hard state other features are dominant. In fact the Fe line is the least important feature in the statistical sense (since the addition of other reflection features, such as the Compton hump plus the Fe edge, gave the most important improvement of the fit). We also find very similar inner disk radii in the hard and soft state, indicating that the inner disk rim does not change significantly at different spectral states down to a luminosity of $\sim 3\%$ the Eddington limit.

REFERENCES

Ballantyne D. R., 2004, MNRAS, 351, 57

Barret D., Olive J.-F., 2002, ApJ, 576, 391

Barret D., Olive J. F., Boirin L., Done C., Skinner G. K., Grindlay J. E., 2000, ApJ, 533, 329

Barrio F. E., Done C., Nayakshin S., 2003, MNRAS, 342, 557

Beloborodov A. M., 1999, ApJ, 510, L123

Bhattacharyya S., Strohmayer T. E., 2007, ApJ, 664, L103

Boldt E., Leiter D., 1987, ApJ, 322, L1

Cackett E. M., Altamirano D., Patruno A., Miller J. M., Reynolds M., Linares M., Wijnands R., 2009, ApJ, 694, L21

Cackett E. M., Miller J. M., 2013, ApJ, 777, 47

Cackett E. M., Miller J. M., Ballantyne D. R., Barret D., Bhattacharyya S., Boutelier M., Miller M. C., Strohmayer T. E., Wijnands R., 2010, ApJ, 720, 205

Cackett E. M., Miller J. M., Bhattacharyya S., Grindlay J. E., Homan J., van der Klis M., Miller M. C., Strohmayer T. E., Wijnands R., 2008, ApJ, 674, 415

Cackett E. M., Miller J. M., Reis R. C., Fabian A. C., Barret D., 2012, ApJ, 755, 27

D'Aì A., di Salvo T., Ballantyne D., Iaria R., Robba N. R., Papitto A., Riggio A., Burderi L., Piraino S., Santangelo A., Matt G., Dovčiak M., Karas V., 2010, A&A, 516, A36

D'Aì A., Iaria R., Di Salvo T., Matt G., Robba N. R., 2009, ApJ, 693, L1

Dauser T., Wilms J., Reynolds C. S., Brenneman L. W., 2010, MNRAS, 409, 1534

Di Salvo T., D'Aí A., Iaria R., Burderi L., Dovčiak M., Karas V., Matt G., Papitto A., Piraino S., Riggio A., Robba N. R., Santangelo A., 2009, MNRAS, 398, 2022

Di Salvo T., Done C., Życki P. T., Burderi L., Robba N. R., 2001, ApJ, 547, 1024

Di Salvo T., Iaria R., Méndez M., Burderi L., Lavagetto G., Robba N. R., Stella L., van der Klis M., 2005, ApJ, 623, L121

Done C., Gierliński M., Kubota A., 2007, The Astronomy and Astrophysics Review, 15, 1

Egron E., di Salvo T., Burderi L., Papitto A., Barragán L., Dauser T., Wilms J., D'Aì A., Riggio A., Iaria R., Robba N. R., 2011, A&A, 530, A99

Egron E., Di Salvo T., Motta S., Burderi L., Papitto A., Duro R., D'Aì A., Riggio A., Belloni T., Iaria R., Robba N. R., Piraino S., Santangelo A., 2013, A&A, 550, A5

Esin A. A., McClintock J. E., Narayan R., 1997, ApJ, 489, 865

Fabian A. C., Rees M. J., Stella L., White N. E., 1989, MNRAS, 238, 729

Fiocchi M., Bazzano A., Ubertini P., Zdziarski A. A., 2007, ApJ, 657, 448

García J., Dauser T., Lohfink A., Kallman T. R., Steiner J. F., McClintock J. E., Brenne-
man L., Wilms J., Eikmann W., Reynolds C. S., Tombesi F., 2014, ApJ, 782, 76

García J., Kallman T. R., 2010, ApJ, 718, 695

Hasinger G., van der Klis M., 1989, A&A, 225, 79

Iaria R., D'Aí A., di Salvo T., Robba N. R., Riggio A., Papitto A., Burderi L., 2009, A&A,
505, 1143

Kolehmainen M., Done C., Díaz Trigo M., 2011, MNRAS, 416, 311

Koyama K., Tsunemi H., Dotani T., Bautz M. W., Hayashida K., et al. 2007, PASJ, 59, 23

Lin D., Remillard R. A., Homan J., 2010, ApJ, 719, 1350

Magdziarz P., Zdziarski A. A., 1995, MNRAS, 273, 837

Markoff S., Nowak M. A., Wilms J., 2005, ApJ, 635, 1203

Matt G., Perola G. C., Piro L., Stella L., 1992, A&A, 257, 63

Merloni A., Fabian A. C., Ross R. R., 2000, MNRAS, 313, 193

Miller J. M., D'Aì A., Bautz M. W., Bhattacharyya S., Burrows D. N., Cackett E. M.,
Fabian A. C., Freyberg M. J., Haberl F., Kennea J., Nowak M. A., Reis R. C., Strohmayer
T. E., Tsujimoto M., 2010, ApJ, 724, 1441

Miller J. M., Parker M. L., Fuerst F., Bachetti M., Barret D., et al. 2013, ApJ, 779, L2

Mitsuda K., Bautz M., Inoue H., Kelley R. L., Koyama K., et al. 2007, PASJ, 59, 1

Ng C., Díaz Trigo M., Cadolle Bel M., Migliari S., 2010, A&A, 522, A96

Olive J.-F., Barret D., Gierliński M., 2003, ApJ, 583, 416

Pandel D., Kaaret P., Corbel S., 2008, ApJ, 688, 1288

Papitto A., D'Aì A., Di Salvo T., Egron E., Bozzo E., Burderi L., Iaria R., Riggio A.,
Menna M. T., 2013, MNRAS, 429, 3411

Papitto A., Di Salvo T., D'Aì A., Iaria R., Burderi L., Riggio A., Menna M. T., Robba
N. R., 2009, A&A, 493, L39

Papitto A., Riggio A., di Salvo T., Burderi L., D'Aì A., Iaria R., Bozzo E., Menna M. T.,
2010, MNRAS, 407, 2575

Piraino S., Santangelo A., di Salvo T., Kaaret P., Horns D., Iaria R., Burderi L., 2007,
A&A, 471, L17

Piraino S., Santangelo A., Ford E. C., Kaaret P., 1999, A&A, 349, L77

Piraino S., Santangelo A., Kaaret P., Mück B., D'Aì A., Di Salvo T., Iaria R., Robba N.,

Burderi L., Egron E., 2012, A&A, 542, L27

Reis R. C., Fabian A. C., Miller J. M., 2010, MNRAS, 402, 836

Reis R. C., Fabian A. C., Young A. J., 2009, MNRAS, 399, L1

Ross R. R., Fabian A. C., 2005, MNRAS, 358, 211

Ross R. R., Fabian A. C., Young A. J., 1999, MNRAS, 306, 461

Sanna A., Hiemstra B., Méndez M., Altamirano D., Belloni T., Linares M., 2013, MNRAS, 432, 1144

Shaposhnikov N., Titarchuk L., Laurent P., 2009, ApJ, 699, 1223

Takahashi T., Abe K., Endo M., Endo Y., Ezoe Y., et al. 2007, PASJ, 59, 35

Tomsick J. A., Yamaoka K., Corbel S., Kaaret P., Kalemci E., Migliari S., 2009, ApJ, 707, L87

van der Klis M., 2006, Advances in Space Research, 38, 2675

van Paradijs J., McClintock J. E., 1994, A&A, 290, 133

Yoshida K., Mitsuda K., Ebisawa K., Ueda Y., Fujimoto R., et al. 1993, PASJ, 45, 605

Young A. J., Fabian A. C., Ross R. R., Tanaka Y., 2001, MNRAS, 325, 1045

Zdziarski A. A., Lubiński P., Smith D. A., 1999, MNRAS, 303, L11

Życki P. T., Done C., Smith D. A., 1999, MNRAS, 309, 561